Phenomenological Combustion Modeling of a Direct Injection Diesel Engine with In-Cylinder Flow Effects

Yong H. Im, Kang Y. Huh*
Department of Mechanical Engineering, Pohang University of Science & Technology

A cycle simulation program is developed and its predictions are compared with the test bed measurements of a direct injection (DI) diesel engine. It is based on the mass and energy conservation equations with phenomenological models for diesel combustion. Two modeling approaches for combustion have been tested; a multi-zone model by Hiroyasu et al (1976) and the other one coupled with an in-cylinder flow model. The results of the two combustion models are compared with the measured imep, pressure trace and NOx and soot emissions over a range of the engine loads and speeds. A parametric study is performed for the fuel injection timing and pressure, the swirl ratio, and the squish area. The calculation results agree with the measured data, and with intuitive understanding of the general operating characteristics of a DI diesel engine.

Key Words : Cycle Simulation, Direct Injection Diesel Engine, Phenomenological Combustion Model, Multi-Zone, In-Cylinder Flow

Nomenclature

C_f, C_p, C_r, C_e	: Correction factor
C_{pg}	: Specific heat at constant pressure
$C_{\varepsilon 1}, C_{\varepsilon 2}$	: Constant for turbulence model, dimensionless
C_k, C_l, C_d	: Constnats for inlet flow turbulence, dimensionless
d_{32}	: Sauter's mean diameter
F_κ	: Boundary flux of κ
F_ε	: Boundary flux of ε
h	: Enthalpy/convective heat transfer coefficient
h_{fg}	: Heat of vaporization
I	: Angular momentum
k_g	: Thermal conductivity
L_v	: Valve lift
N	: Number of droplets in the package
ΔP	: Difference between injection pressure and cylinder pressure
r_s	: Swirl ratio
r_b	: Cup radius
S	: Spray tip penetration
S_l	: Laminar flame speed
t_b	: Breakup time
T	: Temperature
T_s	: Torque
u	: Specific internal energy
u'	: Turbulent fluctuation velocity
V_θ, V_r	: Velocity in polar coordinates
V	: Volume

Greek Letters

α, β, γ	: Parameters in velocity profiles, dimensionless
κ	: Turbulent kinetic energy
ε	: Turbulence dissipation rate
τ_c	: Turbulent combustion time scale
τ_e	: Turbulent mixing time scale
$\tau_{d,j}$	: Ignition delay for the j-th element

* Corresponding Author,
E-mail : huh@vision.postech.ac.kr
TEL : +82-562-279-2177 ; **FAX** : +82-562-279-3199
Associate Professor, Department of Mechanical Engineering, Pahang University of Science and Technology, San 31, Hyoja-dong, Nam-gu, Pohang 790-784, Kyungbuk, Korea. (Manuscript **Received** October 12, 1999; **Revised** February 22, 2000)

ρ : Density
Ω : Specific angular momentum
ν : Kinematic viscosity
λ : Taylor micro scale
γ : Specific heat ratio
ϕ : Equivalence ratio

1. Introduction

Cycle simulation with phenomenological combustion models has been used as a useful tool for analysis of the performance and emissions of a DI diesel engine. These models have proved to be simple, effective and useful, as compared with multidimensional models which currently take too much computation time to be extended to cycle simulation. Phenomenological combustion modeling of a diesel engine has been an active research area since the early attempts of the single-zone analysis for heat release prediction by Austen et al (1961). However, their efforts had limited applicability because their model was not based on a mechanistic combustion process. Kriger et al (1966) established the procedure to obtain an apparent heat release rate from a measured pressure trace. Lyn (1962) proposed an empirical relationship between the fuel injection rate and the apparent heat release rate in order to establish a link between the fuel injection system and the resulting combustion process.

Multi-zone combustion models may be classified into two groups on the basis of the spray model. In Chiu et al (1976) the fuel spray is modeled as a vapor jet by assuming a supercritical state under normal operating conditions. The fuel vapor concentration distribution is described by appropriate analytical functions from the nozzle exit. Hiroyasu et al (1976) developed a model on the basis of the evaporation rate of a single droplet and the droplet size distribution in the fuel spray. Heterogeneity of the mixture was dealt with by dividing the fuel spray into many independent elements. The combustion process of each element is analyzed as a mixing process between the fuel spray and surrounding air.

The flow field in the cylinder is one of the most important factors to determine the combustion characteristics of a diesel engine. The combustion rate and formation of pollutants are highly dependent on the in-cylinder flow field. Kono et al (1985) proposed a combustion model coupled with the in-cylinder flow model to investigate the engine performance and emissions. The global angular momentum and the integrated k-ε equations were solved as the in-cylinder flow model. Nishida et al (1989) extended their previous work (Hiroyasu et al, 1976) to a simplified three dimensional model by dividing the cylinder chamber into many computational cells to consider the in-cylinder flow. However, these previous phenomenological combustion models (Hiroyasu et al, 1976; Chiu et al, 1976; Kono et al, 1985; Nishida et al, 1989; Xiaobin et al, 1995; Rosli et al, 1997; Chae et al, 1996) leave room for further improvement with respect to the physical submodels and validation of their results for different engine types and operating conditions. In this work the phenomenological multi-zone combustion model of Hiroyasu et al (1976) is implemented in its own form and in a form combined with the in-cylinder flow model for comparison with the test bed data of a turbocharged DI diesel engine. The main objective here is to provide a reliable and versatile computational tool to predict the performance and emissions with respect to the major design parameters and operating conditions of a DI diesel engine.

2. Conservation Equations

The mass and energy conservation equations with relevant exchange terms are presented below. Three control volumes, i. e., the cylinder, intake and exhaust manifold/port, are shown in Fig. 1 (a). The intake and exhaust tanks are treated as plenums with known pressures and temperatures. The overall flow chart of the cycle simulation program is given in Fig. 3.

2.1 Conservation of mass

The mass conservation equation is

$$\frac{dm}{dt}=\sum_i(\dot{m}_{i,in}-\dot{m}_{i,out}) \tag{1}$$

where m denotes the total mass in the control

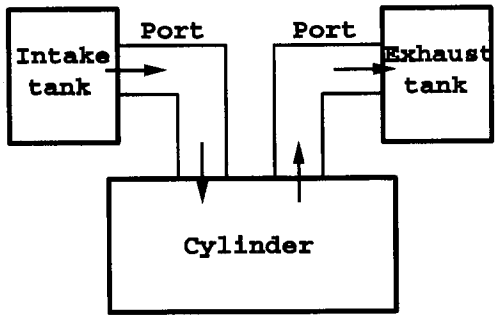

(a) Control volumes

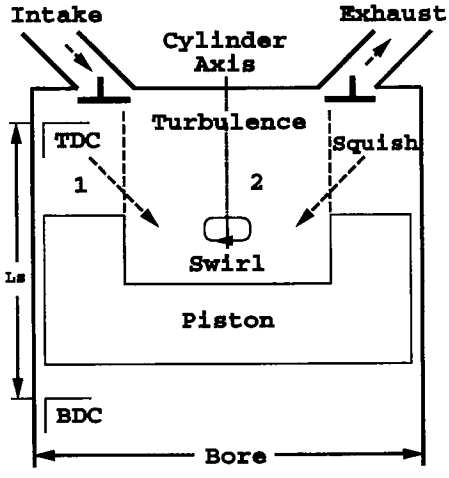

(b) Idealized chamber geometry

Fig. 1 Schematic diagrams for the control volumes and the idealized chamber geometry

volume and $\dot{m}_i$ denotes the mass flow rate in or out through the i-th surface element. A one dimensional quasi-steady compressible flow model is used to calculate the mass flow rate as,

$$\dot{m}=A_e P_1\sqrt{\frac{\psi_1}{R_1 T_1}} \tag{2}$$

$$\psi_1=\frac{2\gamma}{(\gamma-1)}\left[\left(\frac{P_2}{P_1}\right)^{2/\gamma}-\left(\frac{P_2}{P_1}\right)^{\left(\frac{\gamma+1}{\gamma}\right)}\right] \tag{3}$$

where A_e is the effective flow area and γ is the ratio of the specific heats. The pressures, P_1 and P_2, are the upstream and downstream stagnation pressures, respectively. In case the flow through the valve is choked, the critical pressure ratio in the following is used.

$$\left(\frac{P_2}{P_1}\right)_{critical}=\left(\frac{2}{\gamma+1}\right)^{\left(\frac{\gamma}{\gamma-1}\right)} \tag{4}$$

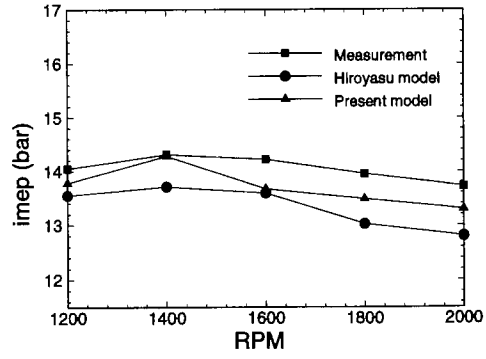

Fig. 2 Comparison of the measured and calculated imep at a full load condition

2.2 Conservation of energy

Application of the first law of thermodynamics to the cylinder gives,

$$\frac{d(mu)}{dt}=-P\frac{dV}{dt}+\sum_i \dot{Q}_i+\sum_i h_i\dot{m}_i \tag{5}$$

where u, P and V denote the average specific internal energy, pressure in the cylinder and cylinder volume. The state in the cylinder is uniquely defined in terms of three independent parameters, P, T, and the equivalence ratio, ϕ. The summations, $\sum_i \dot{Q}_i$ and $\sum_i h_i\dot{m}_i$, denote the net rate of heat transfer and enthalpy flow into the control volume. The convective heat transfer rate to the control volume is expressed as,

$$\dot{Q}_i=\sum_i h_i A_i(T_i-T) \tag{6}$$

where h_i, A_i, and T_i denote the heat transfer coefficient, area, and wall temperature of the i-th surface element. The Woschni's correlation (Woschni, 1967) is used here for the convective heat transfer coefficient. Radiative heat transfer is known to be of negligible importance in the normal operating conditions of a diesel engine. The work done on the piston by the cylinder gas is calculated by integration of the term, pdV, during the whole cycle, while the work during the valve-open period is defined as the pumping work.

3. Combustion Modeling

A phenomenological diesel combustion model

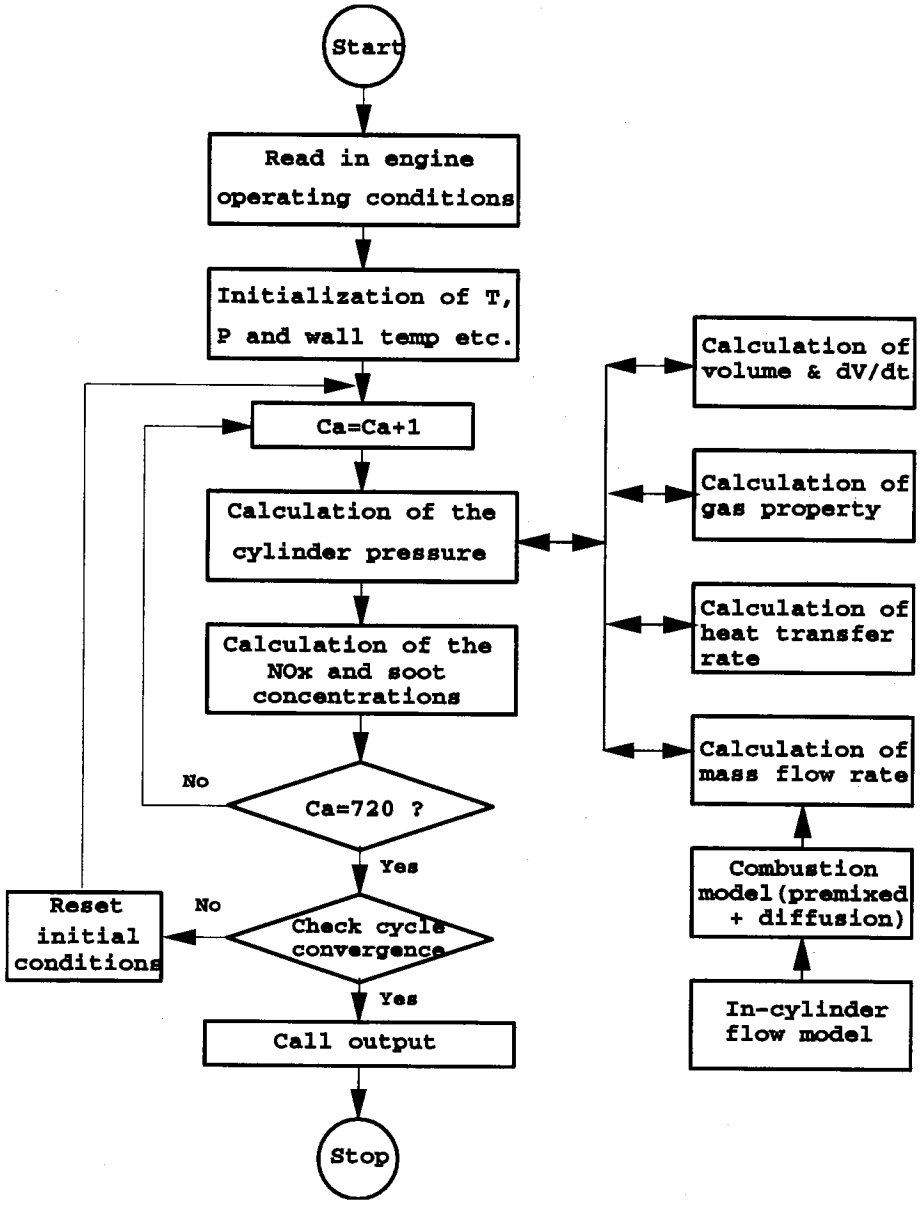

Fig. 3 Flow chart for the cycle simulation

is composed of several submodels for fuel spray and combustion.

3.1 Fuel spray model

3.1.1 Spray penetration

The correlation for the spray penetration by Hiroyasu et al(1983) is used as follows.

$$S=0.39\sqrt{\frac{2\Delta P}{\rho_c}}\cdot t \qquad 0<t<t_b \tag{7}$$

$$S=2.95\left(\frac{\Delta P}{\rho_a}\right)^{1/4}\sqrt{d_o t} \qquad t_b\leq t \tag{8}$$

The spray penetration, S, is in meter and the break-up time, t_b, is given in second as,

$$t_b=28.65\frac{\rho_l d_o}{\sqrt{\rho_a \Delta P}}. \tag{9}$$

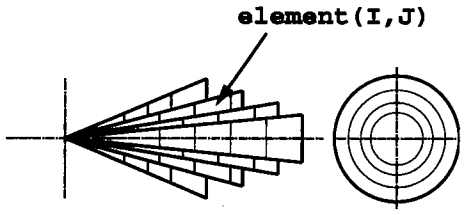

Fig. 4 Schematic of the multi-zone fuel spray

The symbols, ρ_l, ρ_a, d_o and ΔP denote the densities of fuel and cylinder charge in Kg/m^3, the nozzle diameter in meter, and the difference between the cylinder and the injection pressures in Pa.

The spray is divided into many elements with equal mass in the radial and axial directions as shown in Fig. 4. The spray penetration of the (I, J)-th element without swirl is given by an experimental correlation as (Hiroyasu et al, 1983),

$$S_{I,J}=S \cdot exp(-4.403\times10^{-3}(J-1)^2) \quad (10)$$

where I and J denote the index of an element in the axial and radial directions, respectively. The effect of swirl on the spray penetration is accounted for as (Hiroyasu et al, 1983),

$$S_{sw}=(1+\frac{\pi r_s n S}{30 U_o})^{-1} \cdot S \quad (11)$$

$$U_o=0.39(\frac{2\Delta P}{\rho_l})^{1/2} \quad (12)$$

where r_s, n and U_o are the swirl ratio, engine speed in rpm, and injection velocity in m/s at the nozzle exit, respectively.

3.1.2 Air-entrainment model

The rate of entrainment of air into each element is obtained from the principle of momentum conservation. The mass of entrained air during each time step is given as,

$$m_a=m_f \cdot [U_o/(\frac{dS}{dt})-1] \quad (13)$$

where m_f is the total mass of fuel in the element. Matsuoka et al (1989) proposed that re-entrainment of burned gas has significant effects on the diffusion combustion rate. This effect is accounted for as,

$$\dot{m}_{af}=C_f \cdot \dot{m}_a \quad (14)$$

where C_f is an arbitrary constant determined as 0.9 to match the test bed data.

3.1.3 Droplet evaporation model

The d^2-law (Turns, 1993) is used here for the rate of evaporation of a single droplet as,

$$\frac{dD^2}{dt}=-\frac{8k_g}{\rho_l C_{pg}} ln(B_q+1) \quad (15)$$

$$B_q=\frac{C_{pg}(T_\infty-T_b)}{h_{fg}} \quad (16)$$

where k_g, h_{fg} and C_{pg} are the thermal conductivity, heat of vaporization, and specific heat of the gas phase. ρ_l and B_q are the density of the fuel and Spalding's transfer number. T_b and T_∞ denote the boiling temperature of the fuel and the cylinder temperature.

The Sauter mean diameter of the spray is used as the initial droplet diameter (Payri et al, 1988) and given in meter as,

$$d_{32}=2.33\times10^{-3}(\Delta P)^{-0.135}\rho_c^{0.121} V_f^{0.131} \quad (17)$$

where V_f is the fuel volume in m^3 injected per stroke. The pressure difference, ΔP, is in Pa and the density of the cylinder charge, ρ_c, is in Kg/m^3. The mass of the fuel evaporated for a given time step in an element is given by

$$m_{fg}=\frac{\pi}{6}\rho_l(D_{i+1}^3-D_i^3) \cdot N \quad (18)$$

where N is the number of droplets in the element and D_i is the droplet diameter at the i-th time step.

3.2 Combustion model

3.2.1 Ignition delay

The ignition delay for the j-th element of the spray is expressed in second as (Hiroyasu et al, 1983),

$$\tau_{d,j}=C_r P^{-n}\phi^m exp(\frac{E_a}{RT}) \quad (19)$$

where P and T represent the pressure in MPa and the temperature in K in the cylinder. The equivalence ratio, ϕ, is for the given element. The constants C_r, n and m, are chosen to be $C_r=2.0\times10^{-2}$, $n=-2.5$, $m=-1.04$. The activation temperature, E_a/R, is 4000K. It is assumed that ignition

occurs when the following condition is satisfied.

$$\int_{\tau_{inj,j}}^{\tau_{ig,j}} \frac{1}{\tau_{d,j}} dt \geq 1 \tag{20}$$

The integral expression accounts for the variation of pressure and temperature during the ignition delay. The suffix, inj and ig, denote the timing of fuel injection and ignition, respectively.

3.2.2 Premixed combustion

It is assumed that the rate of premixed combustion is proportional to the mass of the fuel-air mixture prepared during the ignition delay period and given as (Kono et al, 1985),

$$\left(\frac{dM_b}{dt}\right)_p = C_p \cdot \left(\frac{M_{mix}}{\tau_c}\right) \tag{21}$$

$$\tau_c = \frac{\lambda}{S_l} \tag{22}$$

where λ is the Taylor microscale and S_l is the laminar flame speed (Tabaczynski et al, 1977). M_{mix} is the mass of the fuel-air mixture in the given element. C_p is an arbitrary tuning constant determined here to be 3.9×10^{-3} to match the test bed data. The Taylor microscale is given as (Tabaczynski et al, 1977),

$$\frac{\lambda}{L} = \left(\frac{15}{A}\right)^{1/2} \left(\frac{u'L}{\nu}\right)^{-1/2} \tag{23}$$

where u' is the turbulent fluctuation velocity, L is the integral length scale, and ν is the kinematic viscosity. The constant, A, is set to be unity. The integral length scale is given in the k-ε model as (Kono et al, 1985)

$$L = C_\nu^{3/4} \frac{k^{3/2}}{\varepsilon} \tag{24}$$

where the constant, C_ν, is 0.09.

3.2.3 Diffusion combustion

Fuel-air mixing is the dominant mechanism to determine the rate of combustion during the diffusion combustion period. The turbulent mixing time scale is introduced to represent the rate of fuel-air mixing as,

$$\left(\frac{dM_b}{dt}\right)_d = \left(\frac{dM_e}{dt}\right) \cdot \left(\frac{\tau_{ca}}{\tau_c}\right) \quad (\tau_{ca} < \tau_c) \tag{25}$$

$$\left(\frac{dM_b}{dt}\right)_d = \left(\frac{dM_e}{dt}\right) \quad (\tau_{ca} > \tau_c) \tag{26}$$

$$\frac{dM_e}{dt} = C_e \cdot \left(\frac{M_e}{\tau_e}\right) \tag{27}$$

$$\tau_e = \left(\frac{L^2}{\varepsilon}\right)^{1/3} \tag{28}$$

where M_b and M_e are the masses of burned fuel and entrained air in the element. The time scales, τ_e and τ_{ca}, denote the mixing time and the time corresponding to one degree crank angle. The arbitrary tuning constant, C_e, is chosen here to be 4.0×10^{-5} to match the test bed data.

The models during the fuel injection period may not be applicable after the end of fuel injection for the spray detached from the nozzle and moving downstream. In the present model with the in-cylinder flow effects, the combustion after the end of fuel injection is described as a mixing process with the available air at a rate controlled by turbulence in the fuel jet as,

$$\frac{dM_e}{dt} = C_{e,a} \cdot \left(\frac{M_{e,a}}{\tau_e}\right) \tag{29}$$

where $M_{e,a}$ is the total mass of unused air in the cylinder. The constant, $C_{e,a}$, is determined from the continuity of the combustion rate at the end of fuel injection. It is clear that combustion after the end of fuel injection may not be treated properly without the in-cylinder flow model (Borgnakke et al, 1981). It is assumed that the combustion rate decreases exponentially after the end of fuel injection (Sato et al, 1982) in the Hiroyasu model (Hiroyasu et al, 1976) without the in-cylinder flow effects.

3.3 In-cylinder flow

The simplified mean flow model of Borgnakke el al (1981) is applied to the mean flow and turbulence in the geometry of a cup-in-piston DI diesel engine. Region '1' is the volume over the piston outside the bowl, and Region '2' is the remaining cylinder volume as shown in Fig. 1(b). The equations of conservation of angular momentum for the two regions are given as,

$$\frac{dI_1}{dt} = T_{s1} + \dot{M}_{in1}\Omega_{in1} - \dot{M}_{12}\Omega_{r_b} \tag{30}$$

$$\frac{dI_2}{dt} = T_{s2} + \dot{M}_{in2}\Omega_{in2} + \dot{M}_{12}\Omega_{r_b} \tag{31}$$

where,

$$I_1=\int\rho\Omega dV_1,\ I_2=\int\rho\Omega dV_2$$
$$\dot{M}_{12}=-2\pi\rho r_b h V_{r_b}$$

The net torque in Regions '1' and '2' are denoted by T_{s1} and T_{s2}, respectively. $\dot{M}_{12}$, Ω, and r_b denote the mass flow rate between the regions, specific angular momentum, and cavity radius, respectively. V_{r_b} and Ω_{r_b} denote the radial velocity and specific angular momentum at the boundary between the two regions. The radial velocity profile is assumed to be,

$$V_\theta=\alpha r+\beta r^2. \tag{32}$$

A uniform turbulence field is assumed with the final equations for the average k and ε obtained by integration over each region as,

$$\rho\frac{dk}{dt}=\frac{2}{3}k\frac{d\rho}{dt}+\overline{P_{sh,k}}-\rho\varepsilon+F_k+\frac{\dot{M}_{in}}{V}(k_{in}-k) \tag{33}$$

$$\rho\frac{d\varepsilon}{dt}=\frac{4}{3}\varepsilon\frac{d\rho}{dt}+\overline{P_{sh,\varepsilon}}-\rho C_{\varepsilon 2}\frac{\varepsilon^2}{k}+F_\varepsilon+\frac{\dot{M}_{in}}{V}(\varepsilon_{in}-\varepsilon) \tag{34}$$

$$\overline{P_{sh,k}}=\frac{\rho\nu_t}{V}\int\left(\frac{\partial V_\theta}{\partial r}-\frac{V_\theta}{r}\right)^2 dV$$
$$\overline{P_{sh,\varepsilon}}=C_{\varepsilon 1}\frac{\varepsilon}{k}\overline{P_{sh,k}}$$
$$k_{in}=(C_k V_{in})^2,\ \varepsilon_{in}=C_d\frac{k_{in}^{3/2}}{C_l L_v}.$$

The symbols, F_k, F_ε and L_v, denote the boundary fluxes of k and ε on the wall (Borgnakke et al, 1981) and the valve lift. The constants, C_d, $C_{\varepsilon 1}$ and $C_{\varepsilon 2}$ are 0.09, 1.45 and 1.9 (Kono et al, 1985). The adjustable constants, C_k and C_l, are chosen here as 0.025 and 0.1, respectively.

3.4 Pollutant emission

3.4.1 NOx

The NOx concentration is calculated by the extended Zeldovich mechanism shown below.

$$O+N_2=NO+N$$
$$N+O_2=NO+O$$
$$N+OH=NO+H \tag{35}$$

By approximating the concentrations of N_2, H, OH, O_2, O by their equilibrium values, it follows that (Heywood, 1988),

$$\frac{d[NO]}{dt}=\frac{2R_1(1-\beta^2)}{\beta R_1/(R_2+R_3)+1} \tag{36}$$

where

$$\beta=\frac{[NO]}{[NO]_{eq}}$$
$$R_1=K_1[O]_e[N_2]_e,$$
$$K_1=7.6\times10^{13}exp[-38000/T]$$
$$R_2=K_2[N]_e[O_2]_e,$$
$$K_2=6.4\times10^9 Texp[-3150/T]$$
$$R_3=K_3[N]_e[OH]_e,\ K_3=4.1\times10^{13}$$

K_1, K_2, and K_3 denote the rate constants for the reactions in Eq. (35). The reaction rates R_1, R_2, and R_3 are in Kmol/m^3s and the temperature, T, is in K.

3.4.2 Soot

The soot formation mechanism is assumed to be a first order reaction of the fuel vapor. The soot oxidation mechanism is assumed to be a second order reaction between the soot and oxygen (Hiroyasu et al, 1983). The net production rate of soot is given as,

$$\frac{dm_s}{dt}=\dot{m}_{sf}-\dot{m}_{sc} \tag{37}$$

$$\dot{m}_{sf}=A_f\cdot m_{fg}\cdot P^{0.5}exp\left(\frac{-E_{sf}}{RT}\right) \tag{38}$$

$$\dot{m}_{sc}=A_c\cdot m_s\cdot\frac{P_{02}}{P}\cdot P^{1.8}exp\left(\frac{-E_{sc}}{RT}\right) \tag{39}$$

where m_s and m_{fg} are the masses of soot and vaporized fuel in the given element. The rates of soot formation and oxidation are denoted by $\dot{m}_{sf}$ and $\dot{m}_{fc}$, respectively. The cylinder pressure and the partial pressure of oxygen are denoted by P and P_{02}. The activation energies, E_{sf} and E_{sc}, are given as 1.25×10^4 *cal/mol* and 1.4×10^4 *cal/mol* (Hiroyasu et al, 1983). The constants, A_f and A_c, are determined from matching the test bed data as $A_f=2.5$ and $A_c=30$.

4. Results and Discussion

The specifications of the test engine and its full-load operating conditions are listed in Table 1 and 2, respectively. Most of the arbitrary model constants are tuned to match the results at the

reference full load condition at 1800 rpm.

4.1 Comparison of Predictions and Measurements

The predicted imep's are compared with the measurements at the full load condition in Fig. 2. The present model with the in-cylinder flow effects shows a slightly better agreement than the Hiroyasu model without the in-cylinder flow effects. The pressure traces by the present model and the Hiroyasu model are compared with the measured ones in Fig. 5 and 6. The rates of fuel burning by the two models are also compared under various operating conditions in Fig. 5 and 6. Note that the present model predicts a slower increase in the fuel burning rate than the Hiroyasu model during the initial stage of combustion. It is due to the different treatment of the premixed fuel-air mixture prepared during the ignition delay period. All of the fuel-air mixture is assumed to burn at ignition in the Hiroyasu model, while the rate of fuel burning in the premixed combustion phase is determined by the laminar flame speed and the Taylor microscale in the present model Eq. (21). The peak pressure from the present model is lower than that from the Hiroyasu model since the peak fuel burning rate is retarded by a few crank angle degrees in the present model. Note also that the present model produces a higher fuel burning rate with a shorter burning duration after the end of fuel injection. The difference is due to the different treatment of the diffusion-controlled combustion (Eq. (29)) in the present model. The combustion rate is assumed to decay exponentially after the end of fuel injection in the Hiroyasu model without the in-cylinder flow effects. The overall agreement between the predicted and measured pressure traces is good for both models with and without the in-cylinder flow effects. The brake specific NOx and soot emissions are compared with the measured data at a full load condition in Fig. 7. The brake specific NOx and soot emissions remain approximately constant or show a minor variation as the engine speed increases. They show good agreement in both the absolute magnitude and the tendency of variation in Fig. 7. Minor underprediction in Fig. 7 may be due to the inaccurate prediction of the temperature for each element in the multi-zone spray or other reasons such as prompt NO which is not taken into account in this simulation. The brake specific NOx emission at 2000 rpm shows some deviation possibly due to a higher friction loss and a lower bmep at a higher rpm. Variation of the NOx and soot concentrations are shown with vs. the crank angle in Fig. 8. Note that the full-load NOx concentration decreases as the engine speed

Table 1 Engine specification

Parameter	Specification
Maximum output	158 kW/2200rpm
Type	6 cylinder 4 cycle direct injection
Bore×Stroke	123 mm×155 mm
Charging type	Turbocharged
Compression ratio	17.1

Table 2 Test conditions (full load)

Parameter	1200 rpm	1400 rpm	1600 rpm	1800 rpm	2000 rpm
Injection start (BTDC)	6	6	7	7	10
Injection end (ATDC)	17	21	19	20	18
Injection pressure (bar)	421	450	577	660	731
Fuel/Stroke (mm^3)	165.58	162.8	160	156.9	152.2
Boost pressure (bar)	0.742	0.939	1.117	1.347	1.487
Air/Fuel ratio	20.49	22.5	24.46	26.77	28.42
Air mass flow rate (kg/h)	629	789	955	1157	1326

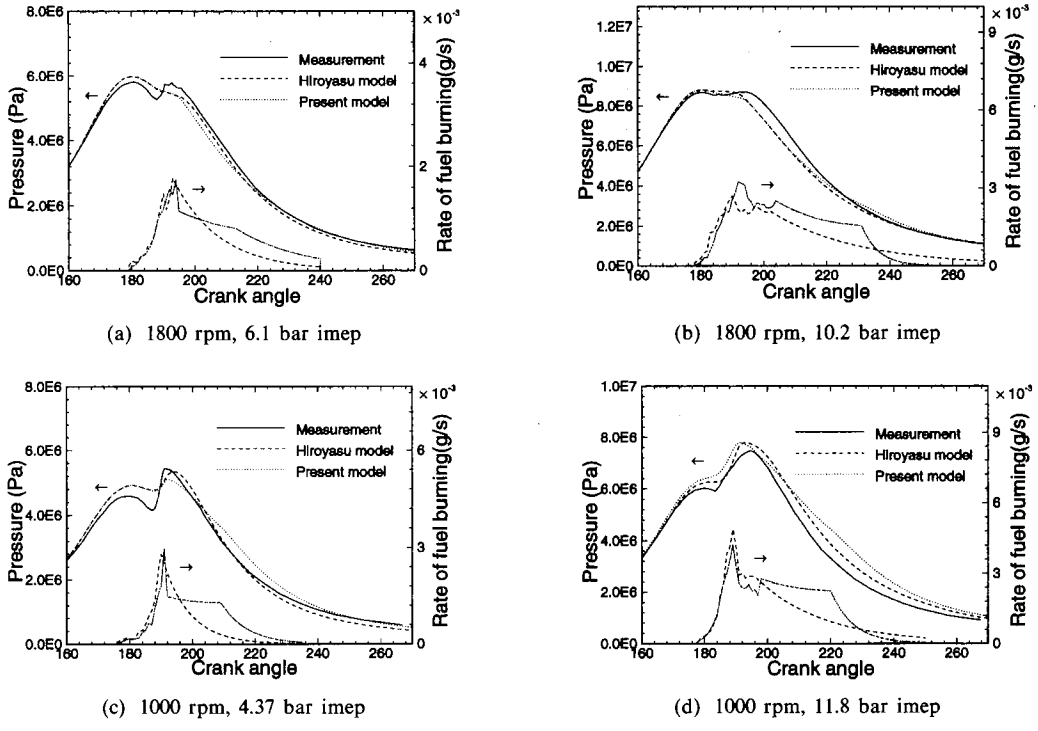

(a) 1800 rpm, 6.1 bar imep (b) 1800 rpm, 10.2 bar imep

(c) 1000 rpm, 4.37 bar imep (d) 1000 rpm, 11.8 bar imep

Fig. 5 Comparison of the measured and calculated pressure trace with the rate of fuel burning (part load)

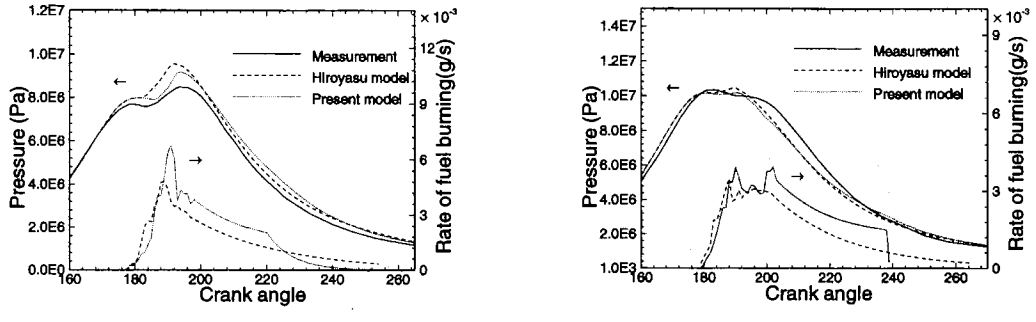

(a) 1200 rpm, 13.8 bar imep (b) 1800 rpm, 13.48 bar imep

Fig. 6 Comparison of the measured and calculated pressure trace with the rate fuel burning (full load)

increases. It is because of a larger full-load imep and a higher peak temperature at a lower rpm in this range of the engine speed. Note also that the soot concentration increases as the engine load increases at a fixed rpm. The NOx concentration tends to be frozen instead of following the equilibrium values in the latter part of the expansion stroke in Fig. 8(a). It is shown in Fig. 8(b) that the soot formation process is faster than the oxidation process, resulting in a rapid increase in the soot concentration after ignition. However, the soot oxidation process is faster than the soot formation process, resulting in a decrease in the soot concentration in the latter part of the expansion stroke.

4.2 Parametric study

The sensitivity of present combustion model is investigated with respect to the fuel injection timing and pressure. The effects of the swirl ratio and squish area are also investigated for the in-cylinder flow effects. Calculations are performed at 1200 rpm and full load conditions.

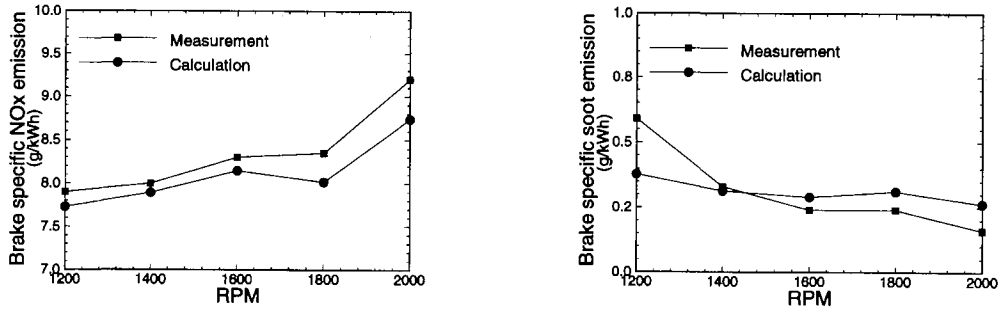

(a) NOx (b) Soot

Fig. 7 Comparison of the measured and calculated NOx and soot emissions at a full load condition

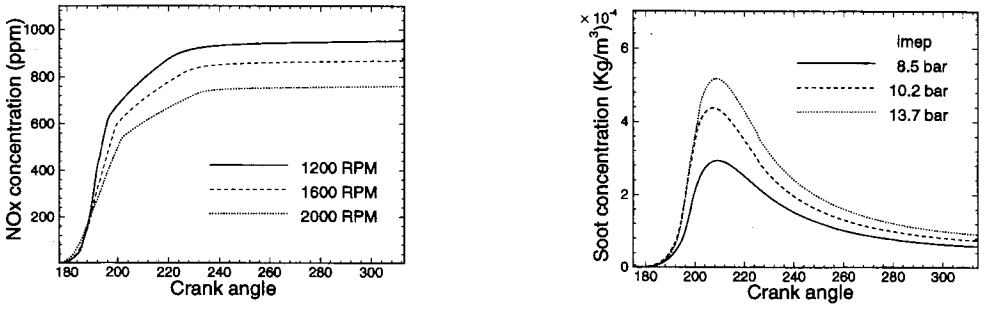

(a) NOx (full load) (b) Soot (part load, 1400 rpm)

Fig. 8 Variation of the NOx and soot concentration with respect to the engine speed and load.

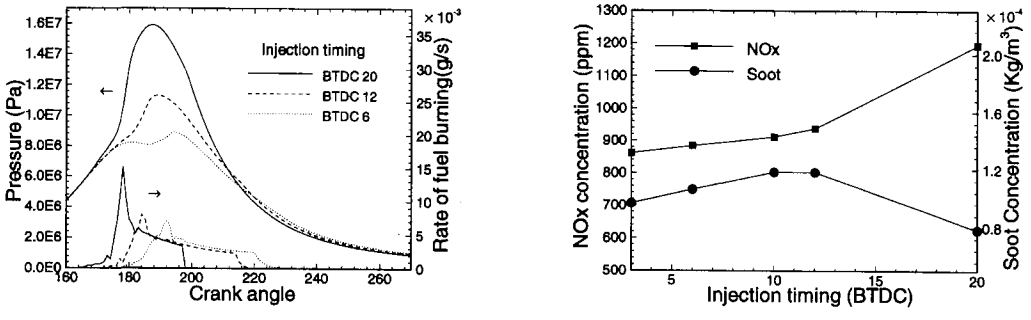

(a) Pressure and rate of fuel burning (b) NOx and soot concentration

Fig. 9 Effects of the injection timing on the cylinder pressure and emissions (full load, 1200 rpm)

4.2.1 Injection timing

Figure 9 shows the effects of the fuel injection timing on the cylinder pressure, rate of fuel burning, and pollutant emissions. An advance in the fuel injection timing increases the peak pressure with an increase in the NOx concentration in Fig. 9(b). The diagram for the rate of fuel burning shows that the amount of the fuel burning in the premixed combustion period increases, resulting in a shorter overall burning duration as the fuel injection timing is advanced. An early fuel injection timing results in a longer ignition delay and an increased amount of premixed fuel-air mixture. An advance in the fuel injection timing, on the other hand, decreases the soot concentration in Fig. 9(b). It is shown in the results that a higher thermal efficiency and a lower NOx concentration cannot be obtained simultaneously. The optimal fuel injection timing in this case may be between BTDC 12 degrees and BTDC 6 degrees. In that range the NOx and soot concentrations remain approximately constant while an

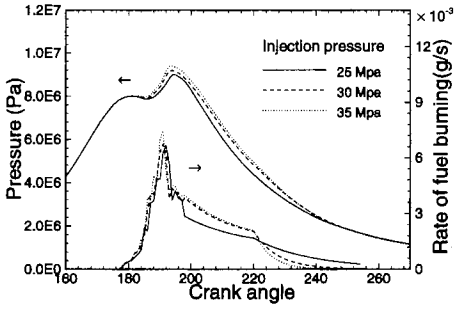

(a) Pressure and rate of fuel burning

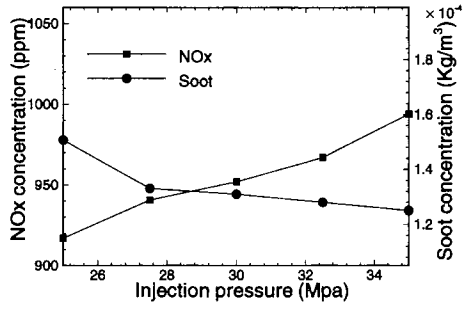

(b) NOx and soot concentration

Fig. 10 Effects of the injection pressure on the cylinder pressure and emissions (full load, 1200 rpm)

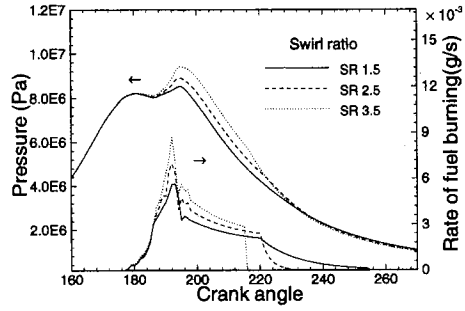

(a) Pressure and rate of fuel burning

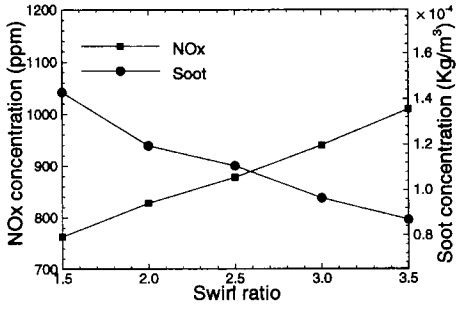

(b) NOx and soot concentration

Fig. 11 Effects of the swirl ratio on the cylinder pressure and emissions (full load, 1200 rpm)

advanced injection timing leads to a relatively high thermal efficiency.

4.2.2 Injection pressure

A higher fuel injection pressure is one of the methods to achieve rapid mixing of the injected fuel with air, which leads to a higher thermal efficiency and a lower soot concentration in a DI diesel engine. Figure 10 shows the effects of the fuel injection pressure on the cylinder pressure, the rate of fuel burning and the pollutant emissions. The injected fuel atomizes into smaller droplets with an increase in the fuel evaporation rate at a higher injection pressure. It accelerates the fuel-air mixing process with an increased amount of premixed fuel-air mixture during the ignition delay period. As a result, a higher injection pressure leads to a shorter burning duration, although the sensitivity of the pressure trace is much less than that of the injection timing in Fig. 10(a). A higher injection pressure leads to a higher peak pressure and temperature to result in a higher NOx concentration and a lower soot concentration as shown in Fig. 10(b).

4.2.3 Swirl ratio

Figure 11 shows the effects of the swirl ratio on the cylinder pressure, rate of fuel burning, and pollutant emissions. The swirling motion in the cylinder plays an important role in determining the mean turbulence level and the rate of fuel-air mixing. Higher swirl motion promotes mixing of the evaporated fuel with air to result in a shorter burning duration. Although the pressure traces show a minor dependence on the swirl ratio in the tested range in Fig. 11(a), a higher swirl ratio leads to a higher NOx concentration and a lower soot concentration in Fig. 11(b). The NOx and soot concentration show an almost linear variation with respect to the swirl ratio in Fig. 11(b).

4.2.4 Squish area

The effects of chamber geometry are investigated for 55, 65 and 75 percent squish areas in Fig.

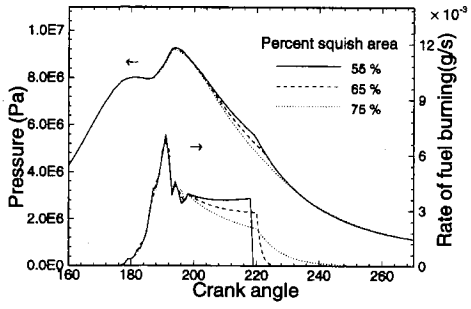

(a) Pressure and rate of fuel burning

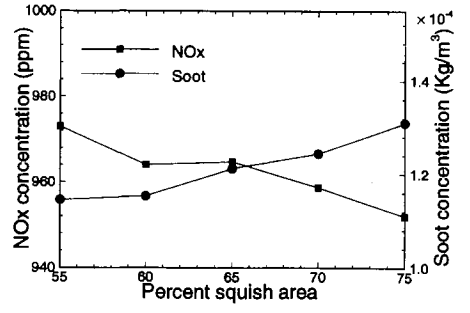

(b) NOx and soot concentration

Fig. 12 Effects of the squish area on the cylinder pressure and emissions (full load, 1200 rpm)

12. The percent squish area is defined as the percentage of the piston area, $\pi B^2/4$, which closely approaches the cylinder head at the end of the compression stroke. Figure 12 shows the effects of the squish area on the cylinder pressure, rate of fuel burning, and pollutant emissions. The pressure trace does not show much dependence on the squish area in Fig. 12(a). In Fig. 12(b) the NOx concentration increases while the soot concentration decreases with a smaller squish area. It may be due to the influence of the integral length scale on the rate of diffusion combustion in Eq. (27). As the squish area increases, the integral length scale increases with an increase in the turbulent mixing time scale. It results in a longer burning duration with a lower thermal efficiency and an increase in the soot concentration. However, variation of the pollutant concentrations are not significant to be within the ± 5 percent in Fig. 12 (b).

5. Conclusion

(1) A cycle simulation program with phenomenological combustion models is developed to predict the performance and emissions of a DI diesel engine. The multi-zone combustion model by Hiroyasu et al is implemented in its own form and in the present form combined with the in-cylinder flow model. The predicted results with the in-cylinder flow model turn out to be in a slightly better agreement with the measurements at various engine operating conditions. Both models give results consistent with the general operating characteristics of a DI diesel engine.

(2) The calculated imep's, pressure traces, and brake specific NOx and soot emissions by the present model are in good agreement with the test bed measurements at full and part load conditions for a range of the engine speeds. However, more validation may be necessary for different engine types and specifications since a few arbitrary model constants are needed to tune the predictions against the measurements.

(3) A parametric study is performed at the full load and 1200 rpm conditions with respect to the fuel injection timing and pressure, swirl ratio, and squish area. The in-cylinder flow model is essential to resolve the dependence on the parameters related to the cylinder flow and chamber geometry. It is shown that the developed program may be used as an auxiliary tool to predict and optimize the combined effects of various engine parameters.

References

Austen, A. E. and Lyn, W. T., 1961, "Some Step toward Calculating Diesel Engine Behavior," SAE paper 409A.

Borgnakke, C., Davis, G. C. and Tabaczynski, R. J., 1981, "Prediction of In-Cylinder Swirl Velocity and Turbulence Intensity for an Open Chamber Cup in Piston Engine," SAE paper 810224.

Chae, J. O., Jianwen, Li, Park, J. K. and Jeong, Y. S. et al, 1996, "A Comparison of Predicted and

Measured Results for a Single-Cylinder DI Diesel Engine at Different Intake Pressure & Composition," Proceedings of the 3rd KSME-JSME Thermal Engineering Conference (I), pp. 323~326.

Chiu, W. S., Shaded, S. M. and Lyn, W. T., 1976, "A Transient Spray Mixing Model for Diesel Combustion," SAE paper 760128.

Heywood, J. B., 1988, *Internal Combustion Engine Fundamentals*, (Singapore: Mcgraw-Hill).

Hiroyasu, H. and Kadota, T., 1976, "Models for Combustion and Formation of Nitric Oxide and Soot in Direct Injection Diesel Engine," SAE paper 760129.

Hiroyasu, H. and Kadota, T., 1983, "Development and Use of a Spray Combustion Modeling to Predict Diesel Engine Efficiency and Pollutant Emissions," *Bulletin of the JSME, 26.*

Kono, S., Nagao, A. and Motooka, H., 1985, "Prediction of In-Cylinder Flow and Spray Formation Effects on Combustion in Direct Injection Diesel Engine," SAE paper 850108.

Kriger, R. B. and Borman, G. L., 1966, "The Computation of Apparent Heat Release for Internal Combustion Engines," *ASME Paper 66-WA/OGP-4.*

Lyn, W. T., 1962, "Study of the Burning Rate and Nature of Combustion in Diesel Engines," *9th Symposium (int ernational) on Combustion*, pp. 1069~1082.

Matsuoka, S. and Yoshizaki, T., 1989, "Model Verification of Burned Gas Re-Entrainment Phenomenon and the Soot Formation Mechanism in Diesel Combustion (Free Spray Flame in Rapid Compression Machine)," SAE paper 89040.

Nishida, K. N. and Hiroyasu, H., 1989, "Simplified Three-Dimensional Modeling of Mixture Formation and Combustion in a D. I. Diesel Engine," SAE paper 890296.

Payri, F. and Benajes, J., 1988, "A Phenomenological Combustion Model for Direct Injection, Compression-Ignition Engines," *APPl. Math. Modelling, Vol. 12.*

Rosli, A. B. and Lee, C. S., 1997, "The Effect of Combustion Parameters on the Nitric Oxide Emission in Direct Injection Type Diesel Engine," KSME Int. J., Vol. 11, No. 6, pp. 672~680.

Sato, G. T. and Tanabe, H. T., 1982, "Study on Diesel Spray and its Combustion," *Proc. XIXth Int. FISTA, No. 82027.*

Tabaczynski, R. J. and Ferguson, C. R., 1977, "A Turbulent Entrainment Model for Spark-Ignition Engine Combustion," SAE paper 770647.

Turns, S. R., 1993, *An Introduction to Combustion*, (Singapore: Mcgraw-Hill), pp. 305~315.

Woschni, G., 1967, "Universally Applicable Equation for the Instantaneous Heat Transfer Coefficient in the Internal Combustion Engine," SAE paper 670931.

Xiaobin, L. and Wallace, J. S., 1995, "A Phenomenological Model for Soot Formation and Oxidation in Direct Injection Diesel Engines," SAE paper 952428.